Corrosion products resulting from carbonation acting upon chloride-induced corrosion in 22 years old blast furnace slag concrete

Nicoletta Russo[1], Emanuele Rossi[2], Timo G. Nijland[3], Rob Polder[4], Federica Lollini[5]

[1] *Department of Chemistry, Materials & Chemical Engineering, Politecnico di Milano, Milan, Italy*

[2] *Department of Civil Engineering, Delft University of Technology, Delft, The Netherlands*

[3] *TNO Buildings, Infrastructure & Maritime, Delft, The Netherlands*

[4] *RPCP, Gouda, The Netherlands*

[5] *Department of Chemistry, Materials & Chemical Engineering, Politecnico di Milano, Milan, Italy*

[1] Email: nicoletta.russo@polimi.it

[2] Email: e.rossi@tudelft.nl

[3] Email: timo.nijland@tno.nl

[4] Email: robpolder@robpolder.demon.nl

[5] Email: federica.lollini@polimi.it

Abstract

The Service life evaluation of reinforced concrete structures is usually limited to initiation of corrosion, whilst in practice corrosion in many structures has already reached the propagation stage. To better understand the processes that lead to the cracking and detachment of concrete cover during this phase, knowledge of corrosion products' development over time is required. This paper investigates corrosion products found in blast furnace slag cement concrete, in which natural carbonation acted upon original chloride-induced corrosion. The sample was cast in 1998, after curing subjected to wet-dry cycles to enhance chloride penetration, and later was exposed to unsheltered outdoor conditions. Corrosion products and textures at the concrete-steel interface and late carbonate veinlets within them have been characterized by a combination of optical microscopy, SEM, Raman spectroscopy and CT scanning.

1 Introduction

Service life design and evaluation of reinforced concrete (RC) structures are usually considered limited to the initiation of corrosion, whilst in practice many structures are already in the corrosion propagation phase [1]. Once corrosion has initiated, progressive accumulation of iron oxides and hydroxides at the steel-concrete interface occurs, an expansive phenomenon which leads to concrete cover cracking and detachment, steps leading to the end of the service life. To better understand the processes occurring during corrosion propagation, useful for capacity assessment of corroding RC structures, knowledge of the development of corrosion products in time at the steel-concrete interface (SCI) as well as inside the concrete matrix, and under realistic exposure conditions, is required. Many studies have been carried out recently on the topic, focusing on samples subjected to accelerated laboratory conditions, which, however, may not be fully representative of what occurs in the field [2], [3].

This paper reports characterization of corrosion products in a concrete made with blast furnace slag cement and reinforced with plain carbon steel bars. The sample was cast in 1998, and was initially subjected to wet-dry cycles to enhance chloride penetration and accelerate corrosion initiation. From the end of the cycles it was exposed to unsheltered outdoor conditions, therefore corrosion propagated naturally for 22 years. Through a combination of different techniques, it was possible to

observe corrosion products and textures at the SCI of two rebars, concrete cracking and late carbonate veinlets within concrete and corrosion deposites. In particular, the corrosion distribution around the whole rebar was observed with CT scanning, while different corrosion product deposites were characterized by a combination of optical microscopy, Scanning Electron Microscopy and Raman spectroscopy.

2 Materials and sample layout

The sample is part of the historic TNO-collection of originally 192 samples cast in 1998 with different cement types (CEM I, II/B-V, III/B and V/A), different water/binder ratios, different corrosion initiation conditions (accelerated carbonation, penetrated chlorides, mixed in chlorides), different exposure for the first 2.5 years (20 °C/80% RH, fog room, outdoors) [4] and the same outdoors exposure for all samples after the first 2.5 years. Concrete beams of 100×100×300 mm were reinforced with unribbed, plain carbon steel rebars (Ø 8 mm), three of them with 10 mm and other three with 30 mm concrete cover (Fig. 1). Samples were also equipped with four stainless steel bars (Ø 6 mm) as resistivity probes at different depths (10 and 50 mm). Finally, two titanium wires were provided as reference electrodes to enable measuring steel potentials.

The sample analysed in this work is part of a study on the nature and development of corrosion products in these samples. The sample was made with CEM III/B 42.5 N (ca. 70% slag) and w/b 0.45, subjected to corrosion initiation by chloride penetration, forced by wet-dry cycles with 3.5% NaCl over 6 months. After the initial chloride exposure, the sample was left in outdoor unsheltered environmental conditions. The sample had an age of 22 years at the point of investigation. During the exposure, natural carbonation reached the upper side of the rebars with concrete cover of 10 mm, as was measured using phenolphthalein. Of these, two rebars, one in sound (uncracked) concrete and one with a corrosion-induced crack, were taken out of the concrete sample, through cores with Ø 20 mm (in red in Figure 1) and investigated.

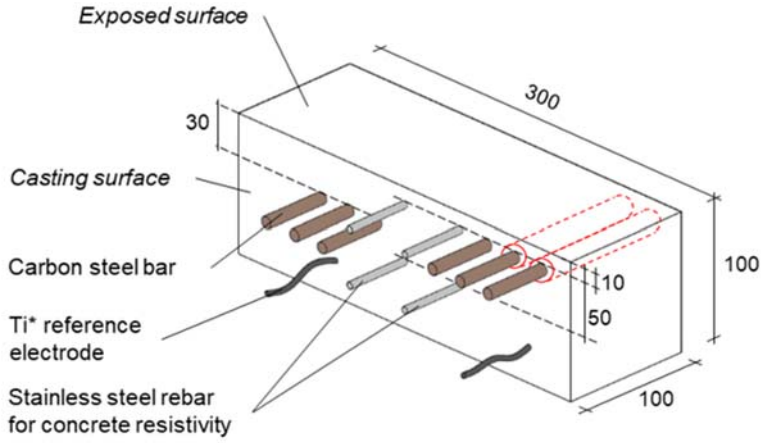

Fig. 1 Sample layout (dimensions in mm).

3 Analytical methods

Corrosion products and textures were studied by a combination of optical microscopy, scanning electron microscopy (SEM), X-ray computed tomography (CT scan) and Raman spectroscopy. Firstly, CT scans were performed on the two cores, over an effective length of 44 mm, in order to visualize the distribution of pits on the whole steel surface, with a spatial resolution (voxel size) of 20 μm. Subsequently, the cores were cut perpendicular to the rebar at several points, to perform optical microscopy, SEM and Raman spectroscopy. Optical microscopy was performed on thin sections in both transmitted and reflective light modes, one thin section including the rebar. On a polished section, SEM was performed using a FEI Nova NanoSEM 650 with a Thermo NSS eFS microanalysis system with Si drift detector at acceleration voltages of 3.5-10 kV. On the same sections, Raman spectrosco-

py was performed in some relevant points, using a Renishaw InVia reflex Raman microscope in the region of 200-1700 cm^{-1}, 60 s acquisition time, using a laser with an excitation wavelength of 532 nm.

4 Results and discussion

The renders of the CT scans are shown in Fig. 2, together with the investigated cores, illustrating the distribution of pits over the steel surface. In the renders, only the scanned portion of the rebar is visible, in four different pictures in order to show the whole steel surface. It can be noticed that after the exposure for 22 years, corrosion has propagated in the form of pits distributed on the whole surface of the bar in the uncracked core. In the cracked core, however, a portion of the steel seems to be more subject to pitting corrosion, with a higher density of several minor pits distributed over the whole length.

Fig. 2 Renders of the steel surface (four images showing four different faces) for the core in sound concrete (left) and the one with an associated crack (right).

Scanning electron microscopy and optical microscopy images of the steel cross sections are reported in Figs 3-7. Combined optical and scanning electron microscopy showed the following corrosion textures:

1. Presence of shallow pits in the steel, and a uniform layer of corrosion products (ISPL) situated between a brighter layer (probably the original mill scale) and the steel surface, (Figs. 3 and 4). Small uncorroded remains of the steel may be present in the corrosion product layer (Fig. 4). This feature was observed in both cores (cracked and uncracked).
2. In the uncraked core, shallow, broad pits filled with corrosion products and with bright marblings towards the outside (Fig. 5). The corrosion product layer in this case does not continue along the steel outside the pit. In the cement paste, corrosion products probably completely filling an air void at the steel concrete interface and further deposited in the cement paste.
3. Only in the uncracked score, a continuous and uniform layer of corrosion products outside the brighter mill scale layer, associated with a probably already existing open concrete-steel interface (Fig. 3).
4. Corrosion products precipitated in the cement paste, beyond the brighter mill scale layer, both in the uncracked (Fig. 5) and in the cracked core (Fig. 4, and also visible in Fig. 7 as brown deposits among the aggregates in concrete).
5. Corrosion products precipitated as euhedral crystals in air voids at the steel-concrete interface, both in the uncracked and cracked cores. In the uncracked core, the air void appeared completely filled with corrosion products, and the euhedral structure is very dense (Fig. 5, right). In the cracked core, corrosion products appeared partly as well defined euhedral crystals growing into the void, partly as layered products on the void walls (Fig. 6).

6. In the cracked core, tiny veinlets of calcium carbonates within the corrosion products in the cracks (Fig. 7) or as disperse precipitate (Fig. 6).

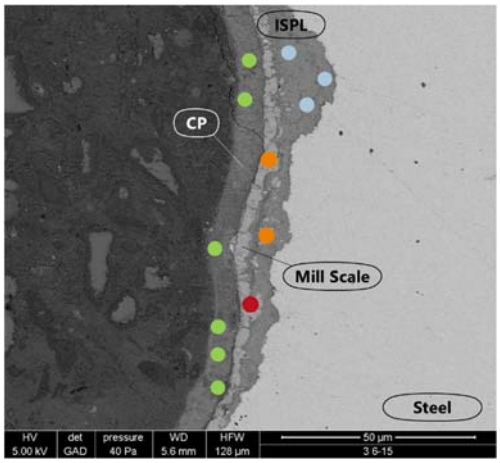

Fig. 3 Raman data superimposed on SEM image, rebar in sound concrete. Green maghemite / ferryhydrite / feroxyhyte, red magnetite, orange wüstite, blue goethite. For discussion, see text.

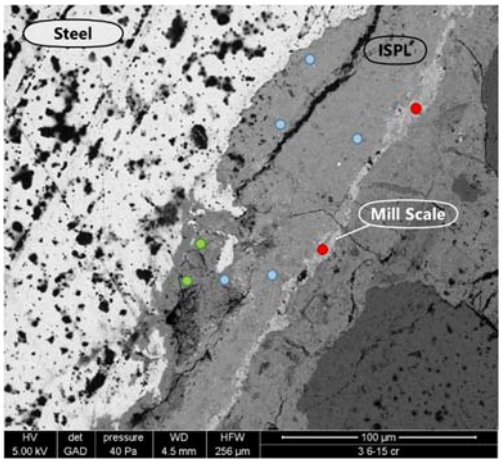

Fig. 4 Raman data superimposed on SEM image, rebar with associated crack. Green maghemite / ferryhydrite / feroxyhyte, red magnetite, blue goethite. For discussion, see text.

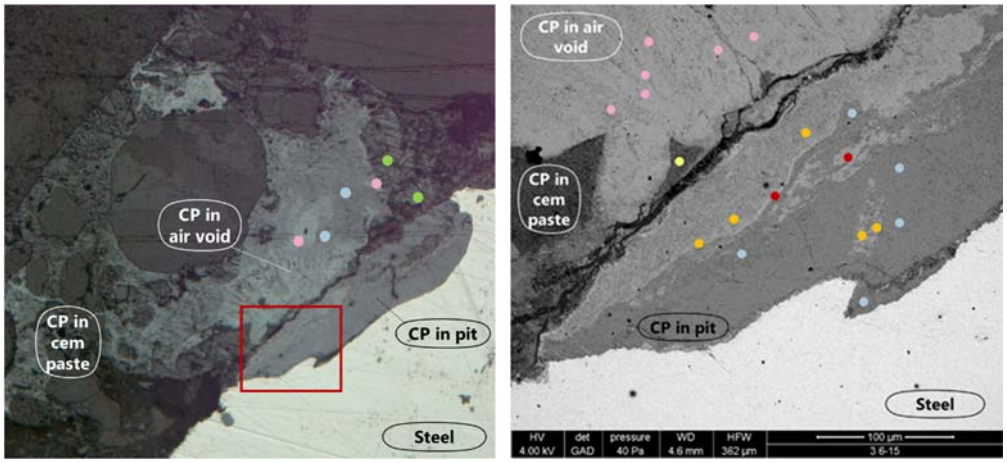

Fig. 5 Raman data superimposed on reflective light (left) and SEM image (right, detail), rebar in sound concrete. Green maghemite / ferryhydrite / feroxyhyte, light green maghemite / ferryhydrite / feroxyhyte and cement paste, pink and orange maghemite, blue goethite, red magnetite. For discussion, see text.

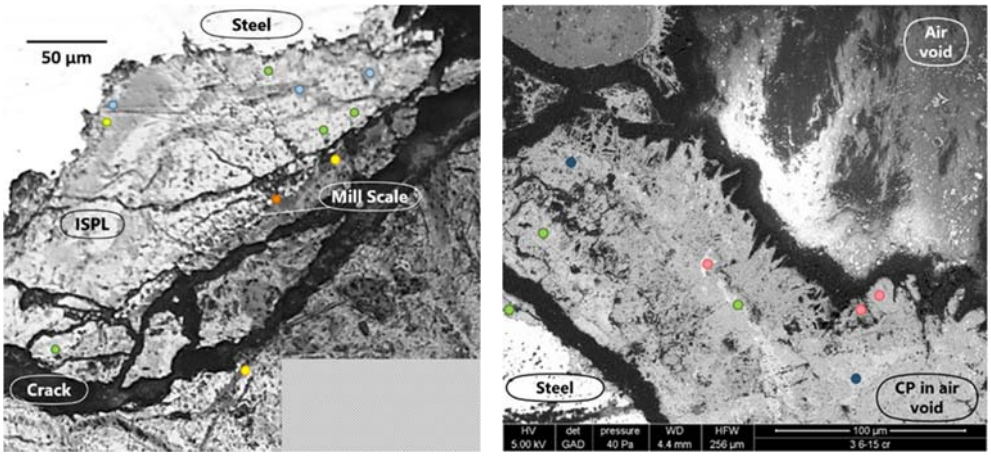

Fig. 6 Raman data superimposed on SEM image, rebar with associated crack. Green maghemite / ferryhydrite / feroxyhyte, light green idem with goethite, orange wüstite, blue goethite, yellow calcium carbonate, dark blue lepidocrocite, pink akaganéite.

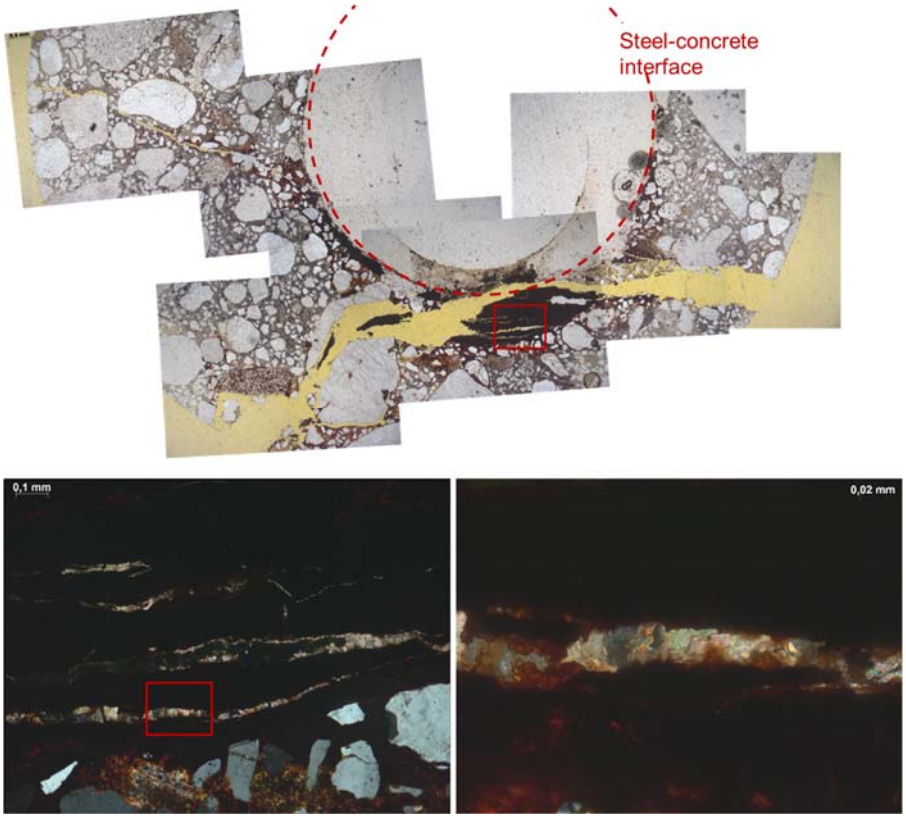

Fig. 7 Transmitted light microphotographs of the rebar with associated crack. The upper picture provides an overview. The lower pictures show the tiny veinlets of calcium carbonate within the corrosion products.

Table 1 Mineralogy of corrosion products.

	Akaganéite	Ca-carbonate	Goethite	Lepidocrocite	Maghemite	Maghemite / Ferrihydrite / Feroxyhyte	Magnetite	Wüstite
Mill scale							X	X
Pit			X			X		
Uniform product layer, within mill scale (outer shell)					X			
Marblings in uniform product layer, within mill scale					X	X		X
Uniform product layer, outside mill scale						X		
Disperse precipitates in cement paste					X	X		
Precipitates in cracks		X						
Precipitates in air voids	X			X	X			

Minerals: akaganéite, $Fe_8(OH,O)_{16}Cl_{1.25}{\cdot}nH_2O$, Ca-carbonate $CaCO_3$, ferrihydrite $Fe_{10}O_{14}(OH)_2$, feroxyhyte δ-FeOOH, goethite α-FeOOH, lepidocrocite γ-FeOOH, magnetite, Fe_3O_4, maghemite γ-Fe_2O_3, wüstite FeO

It is well known and accepted that corrosion induces cracks in the concrete cover, and the subsequent concrete cover detachment (spalling). In particular, the formation of corrosion products implies an increase in the initial volume occupied by iron, from 2 to 6 times greater depending on the type of iron oxide or iron hydroxide that is formed [1]. This expansive process causes internal stresses at the steel-concrete interface which, once the tensile strength of the concrete is exceeded, leads to cracking phenomena. It is therefore important to investigate which type of iron oxide or iron hydroxide is formed, depending on the specific local conditions (exposure conditions, steel-concrete interface, presence of cracks…), since, together with the concrete properties (tensile strength, presence of air voids, …), will be useful for attempts at modelling the cracking of the concrete cover.

In this study, the nature of the corrosion products, in relation to the different textures, has been investigated with Raman spectroscopy, and is also indicated in figures 3-6. In the obtained spectra, it is not always possible to distinguish between maghemite, ferrihydrite and feroxyhyte with certainty. Table 1 gives an overview of the occurrence of different Fe-phases versus textures. Combining texture information and Raman analyses, the following observations can be made:

- **Mill scale:** Raman analyses on the brighter layer detected the presence of iron oxides such as magnetite and wüstite, confirming that this layer corresponded to the original mill scale present on the steel surface at the moment of concrete casting [5], [6]. The mill scale textures observed suggested that the pits were located at places where the mill scale was originally damaged, enabling ingress of corrosive agents, and giving rise to crevice corrosion (Figs. 3, 5).
- **Corrosion product layer:** the relative age relationship between the uniform product layer at the inner side of the mill scale and the pit is unclear (Fig. 3): was the pit formed first, the uniform product layer being formed subsequently? This may imply a slower reduction of the cross section of the steel with time. An open question, at least from the present textures, is also whether the maghemite marblings (Fig. 5) represent displaced, oxidized slivers of the mill scale or derive from oxidation of goethite. In the first case, the process would imply an expansion in volume, and subsequent rise in internal stresses, while this would not happen in the second case.
- **Steel concrete interface:** It has been suggested in literature that the presence of defects at the concrete-steel interface (such as voids) plays a role in corrosion initiation and the location of

pitting, although contradicting results have been found [7]-[9]. In this study, results suggested that the presence of an open void at the steel-concrete interface, as can be seen in figure 3, may also modify the mechanism of corrosion. Lack of adhesion between cement paste and steel results in formation of a uniform product layer *outside* the mill scale otherwise not observed (*e.g.* [8]). Moreover, corrosion products tend to accumulate in correspondence of voids at the steel concrete interface, starting from void walls [8]. In this case, the availability of void spaces which could accommodate the volume expansion of corrosion products could decrease internal stresses and therefore the probability of concrete cover cracking. On the other hand, filling of voids could mask the presence of significant internal corrosion as it would delay the presence of visible corrosion-induced cracks on the outer concrete surface.

- **Cracks:** an interesting phenomenon was observed in this study, and occurred only in the cracked sample, *i.e.* the presence of calcium carbonate crystals associated with cracks (Fig. 7). A possible explanation of this phenomenon could be the following. After cracking, external agents such as water and CO_2 penetrated very easily in the cracks. Calcium hydroxide, which was available in large amount in non-carbonated concrete, dissolved in water and reacted with CO_2 in the cracks, leading to a very localized formation of calcium carbonate crystals.
- **Corrosion products in the cement paste:** in all the cores observed, corrosion propagation was associated with precipitation of iron oxides and hydroxides in the porosity of the cement paste. In the uncracked core this phenomenon seemed to occur only in proximity of a void at the steel-concrete interface, where a localized corrosion pit was formed (Fig 5) and not to occur at all in the case where all the corrosion products seemed to be accommodated in the open concrete-steel interface (Fig. 3). In the cracked core at a macroscopic scale (Fig. 7), iron compounds precipitated in the cement paste were mainly detected at the steel concrete interface and at the edges of corrosion-induced cracks.

From a mineralogic point of view, the study shows corrosion products in the uniform product layer and pits being made up by less dense phases, such as goethite (density 4.27-4.29 g dm^{-3} and volume expansion coefficient-VEC around 3). In the cement paste and in smaller amounts in the uniform product layer denser phases were found, such as maghemite (density 4.88 g dm^{-3} and VEC around 2) and dense corrosion products in the original mill scale, wüstite (density 5.7 g dm^{-3}) and magnetite (density 5.2 g dm^{-3}). The least dense ones, akaganéite (density 3.52 g dm^{-3}, VEC 3.5) and lepidocrocite (density 4.03-4.13 g dm^{-3}, VEC around 3) occurred as precipitates in air voids, except in a void completely filled with dense crystals, where maghemite was found. However, whereas the in situ and semi in situ corrosion products were predominantly goethite, those in the cement paste were mostly maghemite, thus with a volume expansion coefficient around 2-3 with respect to iron. However, in Raman spectra, it was not possible to distinguish with certainty feroxyhyte and ferrihydrite, which, among the corrosion products, are characterized by high volume expansion coefficient. The presence of calcium carbonate in cracks demonstrates the presence and mobility of calcium and CO_2.

5 Conclusions

In this study, corrosion products in a reinforced blast furnace slag cement concrete sample, initially subject to chloride penetration and subsequently to natural corrosion propagation over 22 years, were characterized though a combination of different techniques. Two different rebars were analyzed, one in sound concrete and the other with a corrosion-induced crack.

CT scans of the two concrete cores containing the reinforcing bars allowed to display the steel surface and the localization of corrosion attack. In both samples, isolated pits were visible, distributed on the whole steel surface. In the cracked sample, however, one portion of steel seemed to be subject to a higher level of corrosion, with a higher density of pits of smaller dimensions.

The analysis of the SEM images showed that pits tended to originate where the mill scale was previously more damaged, and that in presence of air voids or open steel-concrete interface, corrosion products tended to precipitate there, as euhedral crystals, eventually depositing in the cement paste.

Raman spectroscopy on corrosion products allowed to define the mineralogy of corrosion products. In particular, less dense iron hydroxides as akaganeite and lepidocrocite were mainly found as precipitate in air voids, while mainly goethite and maghemite were found in the corrosion product layer at the steel concrete interface, in all cases with a volume expansion coefficient between 2 and 3.5. No particular difference in the mineralogy of corrosion products was found between the cracked

and the uncracked sample. However, it was not always possible to distinguish between maghemite and feroxyhyte/ferrihydrite by Raman. Finally, with optical microscopy on thin section and with Raman, crystals of calcium carbonate were found in smaller cracks in the concrete and in the corrosion products.

Acknowledgements

The authors would like to acknowledge Johan Bijleveld and Santiago Garcia from the Faculty of Aerospace Engineering, Delft University of Technology, for their assistance with Raman spectroscopy analyses, and TNO Buildings, Infrastructure & Maritime, for the financial support.

References

[1] Bertolini, L., Elsener, B., Pedeferri, P., Redaelli, E. and Polder R. 2013. *Corrosion of steel in concrete: Prevention, diagnosis, repair (2nd ed.).* Weinheim, Germany: Wiley VCH.

[2] Savija, B., Lukovic, M., Hosseini, S.A.S., Pacheco, J. and Schlangen, E. 2015. "Corrosion induced cover cracking studied by X-ray computed tomography, nanoindentation and energy dispersive X-ray spectrometry (EDS)." *Materials and Structures* 48:2043-2062.

[3] Dehoux, A., Bouchelaghem, F. and Berthaud, Y. 2015. "Micromechanical and microstructural investigation of steel corrosion layers of variable age developed under impressed current method, atmospheric or saline conditions." *Corrosion Science* 97:49-61.

[4] Polder, R.B., and Peelen, W.H.A. 2002. "Characterisation of chloride transport and reinforcement corrosion in concrete under cyclic wetting and drying by electrical resistivity." *Cement & Concrete Composites* 24:427-435.

[5] Demoulin, A., Trigance, C., Neff, D., Foy, E., Dillmann, P., L'Hostis, V. 2010. "The evolution of the corrosion of iron in hydraulic binders analysed from 46-and 260-year-old buildings." *Corrosion Science* 52:3168-3179.

[6] Poupard, O., L'Hostis, V., Catinaud, S., Petre-Lazar, I. 2006. "Corrosion damage diagnosis of a reinforced concrete beam after 40 years natural exposure in marine environment." *Cement and Concrete Research* 36:504–520.

[7] Angst, U.M., Geiker, M.R., Alonso, M.C., Polder, R.B., Isgor, B., Elsener, B. Wong, H., Michel, A., Hornbostel, K., Gehlen, C., François, R. Sanchez, M., Criado, M., Sorensen, H., Hansson, C., Pillai, R., Mundra, S., Gulikers, J., Raupach., M., Pacheco, J., Sagüés, A. 2019. "The effect of the steel-concrete interface on chloride induced corrosion initiation in concrete: a critical review by RILEM TC 262-SCI." *Materials and Structures* 52:88.

[8] Rossi, E., Polder, R., Çopuroğlu, O., Nijland, T. & Šavija, B. 2020. "The influence of defects at the steel/concrete interface for chloride induced pitting corrosion of naturally-deteriorated 20-years-old specimens studied through X-ray Computed Tomography." *Construction & Building Materials* 235:117474.

[9] Boschmann Käthler, C., Angst, U.M., Elsener, B. 2018. "Towards understanding corrosion initiation in concrete – influence of local concrete properties in the steel-concrete interfacial zone." Paper presented at 5th International Conference on Concrete Repair, Rehabilitation and Retrofitting, Cape Town, South Africa, November 19-21.